Swider D.J., Browne M.W., Bansal P.K., Kecman V., ***Modelling of Vapour-Compression Liquid Chillers With Neural Networks,*** Journal of Applied Thermal Engineering, Pergamon Press, Volume 21, Issue 3, pp. 311-329, February 2001

MODELLING OF VAPOUR-COMPRESSION LIQUID CHILLERS WITH NEURAL NETWORKS

D. J. Swider, M. W. Browne, P. K. Bansal*, and V. Kecman

Department of Mechanical Engineering, The University of Auckland

Private Bag 92019, Auckland, New Zealand

Abstract

A new approach to steady state modelling of vapour-compression liquid chillers is presented in this paper. The model uses a generalised radial basis function (GRBF) neural network to predict chiller performance. The GRBF chiller model is developed with the objective of requiring only those input parameters that are readily known to the operating engineer, i.e. the chilled water outlet temperature from the evaporator, the cooling water inlet temperature to the condenser, and the evaporator capacity. The GRBF chiller model predicts relevant performance parameters of a chiller, especially the coefficient of performance. The neural network is applied to two different chillers operating at the University of Auckland, New Zealand and the agreement is found to be within ±5 per cent. It is inferred that neural networks, in particular the generalised radial basis function, can be a promising tool for predicting the chiller's performance for fault detection and other diagnosis purposes.

Keywords: chiller; coefficient of performance; model; neural network; radial basis function; steady state

1. Introduction

The best example of a neural network is the human brain. In fact it is the most complex and powerful structure known. Artificial neural networks try to mimic this biological network in order to learn the solution to a physical problem from a given set of examples. From this, an artificial neural network should be able to learn and predict the performance of a system (be it a chiller).

Different models of vapour-compression liquid chillers have been developed in the past few decades as reported by Browne and Bansal [1]. Browne and Bansal [2] developed a steady-state model for centrifugal chillers, which included component models based on physical laws. The model predicted the measured data to within ±10%. Gordon et al. [3] proposed a thermodynamic model that relates the coefficient of performance (COP) to the cooling capacity. This model needed experimental data to express unknown terms with adjustable parameters. The agreement of the

* Corresponding author. E-mail: p.bansal@auckland.ac.nz

model was found to be within a relative root-mean-square error of 0.4% for the COP but the validation was done with the same data set that were used in determining the parameters.

The difficulty with the above two approaches is that they require geometrical parameters of the system that are often not available to the operating engineers (due to reasons of confidentiality). Therefore, another approach of modelling could involve predicting the performance of a chiller without using any physical or thermodynamic models. This paper presents a new kind of steady state model for liquid chillers that considers the system as a black box without requiring information about the internal behaviour. The model is an application of an artificial neural network, and in particular of the generalised radial basis function (GRBF) network. This is a promising field of research and has become increasingly popular in the last few years as neural networks can solve problems much faster than the other approaches.

Numerous applications [4-9] of neural networks related to refrigeration systems can be found in the open literature. However, only a few of them are somehow applicable to chillers and none of them were used for predicting the performance of liquid chillers. In nearly all of the neural network applications in refrigeration systems, multilayer perceptron networks were used and these networks modelled the chiller systems quite well [10-13]. However, only one application of a radial basis function network was found in the open literature for chillers where Haves et al. [14] successfully detected fouling and leakage faults in the cooling coil of an air-handling unit. The Gaussian functions were positioned on a grid of the input space and the standard deviations were selected to be equal to the distance between adjoining centres. No further optimisation of the centre location or standard deviation was implemented and no test method was described.

2. Neural network

Many neural networks have been developed, but the most popular neural networks are known respectively as the multilayer perceptron (MLP) and the generalised radial basis function (GRBF) network. These networks presently form the basis for the majority of practical applications [15], and are therefore the most likely candidates to be applied to chillers for modelling their performance. In this paper, the GRBF network is chosen since it provides several advantages over the MLP network for this application, including [15-16]:

- fast and efficient training methods
- computationally not as intensive
- better approximation properties

The diagram shown in Figure 1 can represent the GRBF network. For most applications the basis functions are chosen to be Gaussian. These Gaussian basis functions are situated between the *input* and *output layer* in the *hidden layer*. The architecture of a generalised radial basis function network has c inputs $x_1,...x_c$ and d outputs $y_1,...y_d$. A total number of **ce** Gaussian functions G_k $(k = 1 \ldots \mathbf{ce})$ compute a localised function of the input vector. The lines connecting the inputs to the Gaussian function represent (a) the elements of the vector $\boldsymbol{\mu}_k$, which describes the location of the centre (in input space) and (b) the elements of the vector $\boldsymbol{\sigma}_k$, which describes the standard deviation of the Gaussian function (in input space). The lines connecting the Gaussian functions to the outputs represent the weights w of the neural network which are comparable to the parameters in the case of curve fitting with simple polynomials. The outputs are then given as a linear combination of the values of the Gaussian functions (see Eq. (3)).

In case of the general N-dimensional case the kth Gaussian function is given as

$$G_k(\mathbf{x}) = \exp\left[-\frac{1}{2}\left((\mathbf{x}-\boldsymbol{\mu}_k)^T \sum\nolimits_k^{-1}(\mathbf{x}-\boldsymbol{\mu}_k)\right)\right], \tag{1}$$

where $\mathbf{x}$ is the N-dimensional input vector and $\boldsymbol{\mu}_k$ is an N-dimensional vector representing the centre location of the kth basis function. The symbol $\sum_k^{-1}$ is the symmetric $N \times N$ covariance matrix of the kth basis function and represents the standard deviation:

$$\sum\nolimits_k^{-1} = \begin{bmatrix} \frac{1}{\sigma_{1k}^2} & \cdots & 0 \\ \vdots & \ddots & \vdots \\ 0 & \cdots & \frac{1}{\sigma_{Nk}^2} \end{bmatrix} \tag{2}$$

The basis function parameters ie. the location of the centres and their number, and the standard deviation, are processed in the *hidden layer training*. The output is given as a linear superposition of basis functions, in the form

$$y(\mathbf{x}) = \sum_{k=1}^{\mathbf{ce}} G_k(\mathbf{x}) \cdot \mathbf{w}_k \,. \tag{3}$$

The weights in the vector $\mathbf{w}$ are subsequently determined in the *output layer training* after the basis function parameters are chosen with use of the sum-of-least squares error function. This error function can generally be written in matrix notation as follows:

$$\mathrm{E} = \frac{1}{2}\left(\mathbf{G} \cdot \mathbf{w}^T - \mathbf{T}\right)^2 \tag{4}$$

where matrix **G** represents all basis functions $G_k(\mathbf{x})$, vector **w** all weights w_k, and the matrix **T** represents all target values (e.g. the measured data patterns). The error function is minimised when the derivative equals zero which has a unique solution for the weights given by

$$\mathbf{w}^T = \left(\left(\mathbf{G}^T\mathbf{G}\right)^{-1}\mathbf{G}^T\right)\mathbf{T} = \mathbf{G}^{-1}\mathbf{T} \tag{5}$$

where $\mathbf{G}^{-1}$ is the pseudo-inverse of the matrix **G**.

3. Description of the chillers

The model is applied to two different hermetic vapour-compression liquid chillers, namely a single-circuited single-screw (Chiller A) and a twin-circuited twin-screw (Chiller B). These chillers are part of a recently (1998) commissioned commercial chilling system for one of the complexes at the University of Auckland, New Zealand. The complex consists of three buildings with a total cooling area of approximately 30,000 m^2. The cooling capacity in each of the chillers is mainly controlled by the chilled water outlet temperature. Typical design conditions for the water temperatures are 6°C for the chilled water outlet temperature and 29°C for the cooling water inlet temperature. Table 1 summarises the general details of the chillers.

4. Experimental Data

Experimental data were collected on both the chillers for the mass flow rates and the inlet and outlet temperatures respectively of chilled and cooling water, and for the electrical work input to the compressor. The cooling water mass flow rate changed under different combined chiller operations. The chilled water mass flow rate was found to be nearly constant (±2 per cent), whereas for each chiller operation, an averaged cooling water mass flow rate was assumed. The cooling capacity of the chiller was evaluated using

$$\dot{Q}_e = \dot{m}_{chw} \cdot c_p \cdot (T_{chw}^{in} - T_{chw}^{out}) \ . \tag{6}$$

The coefficient of performance was calculated using

$$COP = \dot{Q}_e / \dot{W} \ . \tag{7}$$

Figures 2 and 3 show that on January 20, 1999, the chillers were operating in highly dynamic mode, particularly the cooling water temperature. To extract the steady-state data from these measurements, only those operating conditions that varied by less than 2 per cent for Chiller A and less than 5 per cent for Chiller B over a 15 minute time period, were used. The higher percentage for Chiller B was necessary to obtain an adequate number of inputs for the model. Representative parts of the 500 extracted steady-state data patterns for Chiller A and of the 380 for Chiller B are respectively given in Tables 2 and 3. The COP curve obtained from the measurements (measured

COP) for Chiller A versus the cooling capacity (part load fraction) follows a linear trend with higher COPs around the full load. The COP curve for Chiller B, however, follows five linear trends as it has two compressors with three operation stages each. The dependence of the COP to the compressor work results in a relatively high but constant COP under all operating conditions. The lowest measured COP under steady-state conditions was as low as 1.6 for Chiller A, while between 3 and 4 for Chiller B [17].

5. Model input and output parameters

The GRBF chiller model is developed with the objective of requiring only those input parameters that are easily available to the operating engineers. These include the cooling capacity (see Eq. (6)), the chilled water outlet, and the cooling water inlet temperatures (3-dimensional input space). The values of the model input parameters are restricted to the range of the values used for training as given in Table 4. Input values beyond the training range can not be modelled with a sufficient accuracy with a GRBF network. The model predicts all relevant performance parameters. These are the chilled water inlet and cooling water outlet temperatures, as well as the coefficient of performance (see Eq. (7)), and the compressor work input (4-dimensional output space).

6. GRBF chiller model

The GRBF chiller model is implemented under MATLAB as this performs matrix operations and offers simple programming features. The GRBF chiller model is separated in three distinctive parts:

1. data pre-processing
2. hidden layer training
3. output layer training and neural network testing

This is performed for 450 of the 500 measured data patterns for Chiller A and for 342 of the 380 measured data patterns for Chiller C. The remaining 50 and 38 data patterns respectively for Chiller A and B are only used for the final validation of the model (see Section 7). The flowchart of the general structure of the GRBF chiller model is explained in Figure 4.

6.1 Data pre-processing

Initially data pre-processing is employed to randomly redefine the structure of the measured data ie. it is used just once with the whole data set before the actual neural network (*GRBFchil*) is started.

6.2 Hidden layer training

The hidden layer training is separated into two steps, namely (a) the optimisation of the Gaussian functions centres and (b) the optimisation of the standard deviations. For both steps various optimisation methods exist, in this work however only the most popular ones are used.

(a) In optimising the centres of the Gaussian functions, firstly it is necessary to determine the total number of the Gaussian functions (**ce**) and secondly the location of the centres in the input space. The number of Gaussian functions is determined by a supervised training process and has to be initially given as an user input. The fastest approach to choose the location of the centres is to set them equal to some subset of the data patterns from the training set. In this case, the first **ce** data patterns were chosen as centres. This approach to the choice of the centres is very fast, and allows the GRBF chiller model to be set up very quickly. Another very popular method but computationally intensive approach used in this application is the *K*-means algorithm. This algorithm associates each Gaussian function with a group of input data patterns, such that the centre of the Gaussian function is given by the mean of the data patterns in the group. This is achieved by an iterative procedure. In this application, the *K*-means algorithm is an optional optimisation method of the initially located Gaussian functions.

(b) The standard deviations are obtained once the locations of the Gaussian functions are determined. One of the most common ways to determine the standard deviations is used in this application. This is to make them equal to the average distance between the Gaussian functions themselves. The standard deviation determines the degree of overlapping of the Gaussian functions. This overlapping is the reason that only a few Gaussian functions can represent the whole input space. Hence, the degree of overlapping has an influence on the performance of the GRBF chiller model. It can be changed by multiplying the standard deviations with the fine-tune parameter **kks**. This parameter has to be determined by supervising the training process, which is automated in the model.

6.3 Output layer training and neural network testing

The optimum number of Gaussian functions **ce** and the optimum standard deviation fine-tune parameter **kks** are determined by dividing the available set of data (in this case 450 and 342 data patterns respectively for Chiller A and B) randomly into a training and a testing set. For the GRBF chiller model, the cross-validation method is used. The set of data patterns is divided randomly into *S* equal sections, where *S* is chosen to be 10. Each considered network, ie. defined by different values for **ce** and **kks**, is then trained (ie. estimation of the weights) on *S-1* of the sections by

programming Eqs. (1) and (5) in the MATLAB-file *GRBFfunc*. The ability of the network to make predictions for new data is tested on the remaining section using Eq. (3) and by computing an error based on the root-mean-square error function. This is repeated for all *S* possible choices and the results of the error function are then averaged. This overall mean testing error can then be used to compare the performance of a GRBF chiller model by changing the Gaussian function parameters. Hence, it is necessary to repeat the whole hidden and output layer training as well as the neural network testing until a good performance (ie. a low value of the overall mean testing error) is achieved with optimised parameters **ce** and **kks**.

The final GRBF chiller model configurations for Chiller A and B are given in Table 5. The main difference in the parameters is that *K*-means algorithm is not needed to optimise the location of the Gaussian functions for Chiller A, however, it improves the performance of Chiller B. That may be due to the different chiller design and the corresponding COP curves. Chiller A is single-circuited and exhibits a nearly linear COP curve over the whole cooling capacity range while Chiller B is twin-circuited and shows an unsteady COP curve (five nearly linear curves) over the cooling capacity. Table 5 also shows that **ce** and **kks** are higher for Chiller A than for Chiller B. One reason may be that the use of the *K*-means algorithm leads to a better distribution of the Gaussian functions in the input space. Therefore, the less Gaussian functions and a decreased degree of overlapping are necessary to represent the data.

7. Results and discussion

The GRBF chiller models were validated with 50 data patterns for Chiller A and 38 data patterns for Chiller B. These data patterns were not used for training or testing the networks, and, hence, are totally independent. Figures 5 to 12 show comparisons between the experimental and the neural network predicted values (of the independent data patterns). Table 6 shows some statistical results for the GRBF chiller model. The statistical methods employed are (see Appendix) the root-mean-square error (rms), the coefficient of variation (cov), and the absolute fraction of variance (r^2).

Figures 5 and 6 compare the predicted and measured chilled water inlet and cooling water outlet temperatures, respectively for Chiller A and B. It can be seen that the GRBF chiller model predicts them to an accuracy within ±0.5 per cent. The root-mean-square error for the chilled water inlet temperatures respectively for Chiller A and B is 0.02 K and 0.01 K and for the cooling water outlet temperatures respectively 0.28 K and 0.57 K. This is about the accuracy of the temperature measurements of ±0.25 K. However, the predicted cooling water outlet temperature shows more

scatter than the chilled water temperature for both the chillers. This is in line with the cooling water temperatures having higher fluctuations (see Figures 2 and 3).

Figures 7 and 8 highlight the predicted and measured compressor work for the chillers. Nearly all (94 per cent for Chiller A and 87 per cent for Chiller B) of the predicted values are within ±5 per cent of the experimental values. The coefficient of variation is less than 1.7 per cent for Chiller A and about 2.7 per cent for Chiller B. This is about the accuracy of the clamp-on current meters of ±2 per cent. The root-mean-square error for work input to both the chillers is about 2 kW, which is quite low compared with the maximum compressor work input of 138 kW for Chiller A and 72 kW for Chiller B. It does, however, appear that at lower loads the GRBF chiller model tends to overestimate the compressor work slightly. This may be due to the reason that most of the data patterns used for training were in the high load region of operation.

Figures 9 and 10 compare the predicted COP with the measured COP. Nearly all (94 per cent for Chiller A and 84 per cent for Chiller B) of the predicted values agree to within ±5 per cent. The coefficient of variation is less than 1.5 per cent for Chiller A and 3.9 per cent for Chiller B and predicts the COP accurately. The scatter in the figures under part load operation is due to the scatter in the measured data used for training.

Figures 11 and 12 show the trends for the measured and predicted COPs versus cooling capacity part load fraction respectively for Chiller A and B. Figure 11 highlights that the COP prediction for Chiller A agrees well under both the high load and part-load operation. It may be viewed from Figure 12 why the accuracy of the GRBF chiller model for Chiller B is not as accurate as for Chiller A. The main reason for the discrepancies between the predicted and the measured values is the scatter in the measured data (see Tables 2 and 3) where on occasions, a lower chilled water outlet temperature has a higher cooling capacity and compressor work input. This is probably due to the variations in the water mass flow rates through both the evaporator, where a constant average flow rate was used to calculated the evaporator capacity, and the condenser for which constant mass flow rates under different combined chiller operations were assumed. It is also possible that the scatter in the measured data may be due to highly unsteady cooling water inlet temperatures.

8. Conclusions

In this paper, a new approach to modelling vapour-compression liquid chillers has been presented. A generalised radial basis function network has been successfully applied to two different chillers.

The neural network predicted the compressor work input and the COP to within ±5 per cent for both the single-circuited Chiller A and the more complex twin-circuited Chiller B. It may be inferred that neural networks and especially the generalised radial basis function network can be applied to vapour-compression liquid chillers and be used to accurately model their performance. The developed GRBF chiller model can easily be applied to other chillers given a sufficient amount of measured steady-state data. Future studies will concentrate on training the GRBF Chiller model in-situ during the measurements and its application to predict the performance for fault detection and other diagnosis purposes.

9. Acknowledgements

D. J. Swider is thankful to the Technical University Berlin, Germany for granting him a scholarship for his studies at the University of Auckland, New Zealand.

Appendix

The statistical methods employed are:

- **rms** : root-mean-square error defined as

$$\mathrm{rms} = \sqrt{\frac{\sum_{m=1}^{n}\left(y_{pre,m} - t_{mea,m}\right)^2}{n}} \tag{A1}$$

- **cov** : coefficient of variation in per cent defined as

$$\mathrm{cov} = \frac{\mathrm{rms}}{\left|\bar{t}_{mea}\right|} \cdot 100 \tag{A2}$$

- $\mathbf{r^2}$: absolute fraction of variance (value of 1 denotes perfect prediction) defined as

$$\mathrm{r}^2 = 1 - \frac{\sum_{m=1}^{n}\left(y_{pre,m} - t_{mea,m}\right)^2}{\sum_{m=1}^{n}\left(t_{mea,m}\right)^2} \tag{A3}$$

where n is the number of data patterns in the independent data set (respectively for Chiller A and B, n_A=50 and n_B=38), $y_{pre,m}$ indicates the predicted, $t_{mea,m}$ is the measured value of one data point m, and $\bar{t}_{mea}$ is the mean value of all measured data points.

Nomenclature

a) Latin Letters

c	number of neural network inputs
ce	total number of Gaussian functions
c_p	specific heat at constant pressure [kJ/kgK]
COP	coefficient of performance
d	number of neural network outputs
E	error
G	Gaussian function
kks	standard deviation fine-tune parameter
$\dot{m}$	mass flow rate [kg/s]
n	number of independent data patterns
N	number of neural network input dimensions
$\dot{Q}_e$	cooling capacity [kW]
S	number of sections for cross-validation method
t	target neural network output
T	temperature [K]
$\dot{W}$	compressor work input [kW]
w	neural network weight
x	neural network input
y	calculated neural network output

b) Greek Letters

μ	Gaussian functions centre location
σ	Gaussian functions standard deviation

c) Subscripts

chw	chilled water
cw	cooling water
in	inlet
mea	measured
out	outlet
pre	predicted

References

[1] **Browne, M.W. and Bansal, P.K.** Challenges in Modelling Vapour-Compression Liquid Chillers. *ASHRAE Transactions*, **104**(1a):474-486, 1998.

[2] **Browne, M.W. and Bansal, P.K.** Steady-State Model of Centrifugal Liquid Chillers. *Int J. Refrig.*, **21**(5):343-358, 1998.

[3] **Gordon, J.M. and Ng, K.C.** Thermodynamic Modeling of Reciprocating Chillers. *J. Appl. Phys.*, **75**(6):2769-2774, 1994.

[4] **Curtiss, P.S., Kreider, J.F., and Brandemuehl, M.J.** Adaptive Control of HVAC Process Using Predictive Neural Networks. *ASHRAE Transactions*, **99**(1):496-504, 1993.

[5] **Peitsman, H.C. and Bakker, V.E.** Application of Black-Box Models to HVAC Systems for Fault Detection. *ASHRAE Transactions*, **102**(1):628-640, 1996.

[6] **Anstett, M. and Kreider, J.F.** Application of Neural Networking Models to Predict Energy Use. *ASHRAE Transactions*, **99**(1):505-517, 1993.

[7] **Curtiss, P.S., Brandemuehl, M.J., and Kreider**, J.F. Energy Management in Central HVAC Plants Using Neural Networks. *ASHRAE Transactions*, **100**(1):476-493, 1994.

[8] **Gibson, G.L.** A Supervisory Controller for Optimization of Building Central Cooling Systems. *ASHRAE Transactions*, **103**(1):486-493, 1997.

[9] **Massie, D.D., Curtiss, P.S., and Kreider, J.F.** Predicting Central Plant HVAC Equipment Performance Using Neural Networks – Laboratory System Test Results. *ASHRAE Transactions*, **104**(1a):221-228, 1998.

[10] **So, A.T.P., Chow, T.T., Chan, W.L., and Tse, W.L.** A Neural-Network-Based Identifier/ Controller for Modern HVAC Control. *ASHRAE Transactions*, **101**(2):14-31, 1995.

[11] **Palau, A., Velo, E., and Puigjaner, L.** Use of Neural Networks and Expert Systems to Control a Gas/Solid Sorption Chilling Machine. *Int J. Refrig.*, **22**(1):59-66, 1999.

[12] **Ferrano, F.J. and Wong, K.V.** Prediction of Thermal Storage Loads Using a Neural Network. *ASHRAE Transactions*, **96**(2):723-726, 1990.

[13] **Kawashima, M., Dorgan, C.E., and Mitchell, J.W.** Hourly Thermal Load Prediction for the Next 24 Houres by Arima, Ewma, LR, and an Artificial Neural Network. *ASHRAE Transactions*, **101**(1):186-200, 1995.

[14] **Haves, P., Salsbury, T.I., and Wright, J.A.** Condition Monitoring in HVAC Subsystems Using First Principles Models. *ASHRAE Transactions*, **102**(1):519-527, 1996.

[15] **Bishop, C.M.** Neural Networks and their Applications. *Rev. Sci. Instrum.*, **65**(6):1803-1832, 1994.

[16] **Kecman, V.** *Learning and Soft Computing*. MIT Press, Cambridge, MA (to be published in 1999).

[17] **Swider, D.J.** Experimental Investigation and Neural Network Modelling of Vapour-Compression Liquid Chillers. *Student Research Project*, University of Auckland, New Zealand, 1999.

Tables

Table 1: General details of the chillers

Chiller	Compressor	Design	Refrigerant	Cooling Capacity [kW]
A	sigle-screw	single-circuited	R-22	650
B	twin-screw	twin-circuited	R-134a	300

Table 2: Steady-state data for Chiller A

T_{chw}^{out} [K]	Cooling capacity [kW]	Compressor work input [kW]	Coefficient of performance (COP)
280.1	174.1	81.6	2.13
280.7	199.0	85.7	2.27
280.4	238.7	89.8	2.64
280.0	284.8	99.2	2.87
279.9	363.0	117.0	3.10
280.2	468.2	131.2	3.57
279.9	483.5	129.0	3.75
281.1	512.0	132.2	3.87
284.3	534.5	132.9	4.02
283.9	555.6	132.9	4.18
284.5	570.2	132.4	4.31
286.2	661.4	133.3	4.96
284.7	669.2	132.5	5.05
286.2	673.4	133.3	5.05
285.4	676.3	132.6	5.10
285.1	678.2	132.3	5.13

Table 3: Steady-state data for Chiller B

T_{chw}^{out} [K]	Cooling capacity [kW]	Compressor work input [kW]	Coefficient of performance (COP)
279.5	93.5	24.5	3.82
279.6	94.3	25.0	3.78
279.7	104.4	32.4	3.22
279.6	106.7	34.0	3.14
279.2	147.1	42.5	3.46
279.0	151.2	42.1	3.60
279.3	152.6	42.0	3.64
279.1	181.1	42.7	4.24
279.7	209.6	61.7	3.40
279.6	210.8	60.8	3.47
280.1	214.0	61.3	3.49
279.6	259.8	68.3	3.81
280.7	267.9	70.7	3.79
282.1	269.9	71.2	3.79
282.4	270.2	72.9	3.71
283.2	276.9	73.1	3.79

Table 4: Range of the GRBF chiller model input parameters for Chiller A and B

input parameters	Chiller A	Chiller B
cooling capacity [kW]	156.4 - 687.7	81.6 - 298.6
chilled water outlet temp. [K]	279.7 - 286.3	278.8 - 283.8
cooling water inlet temp. [K]	299.0 - 305.0	298.5 - 301.9

Table 5: Configuration of the GRBF chiller model parameters for Chiller A and B

	Chiller A	Chiller B
ce (centers)	23	17
km (*K*-means)	0	1
kks (standard deviation)	9,0	0,5

Table 6: Statistical results for the GRBF chiller models for Chiller A and B

	Chiller A			Chiller B		
	rms	cov	r^2	rms	cov	r^2
COP	0.05	1.44%	0.9998	0.14	3.90%	0.9985
$\dot{W}$	2.03 kW	1.67%	0.9997	1.56 kW	2.27%	0.9993
T_{cw}^{out}	0.28 K	0.09%	1.0000	0.57 K	0.19%	1.0000
T_{chw}^{in}	0.02 K	0.01%	1.0000	0.01 K	0.00%	1.0000

Figures

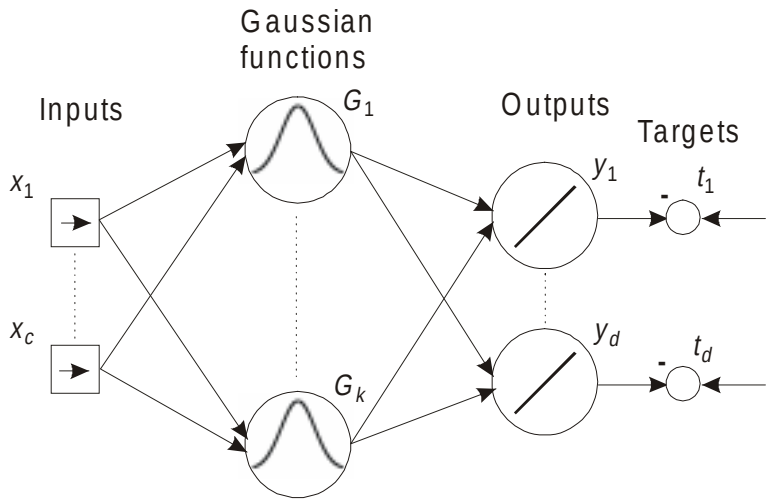

Figure 1: Architecture of a high dimensional in- and output GRBF network

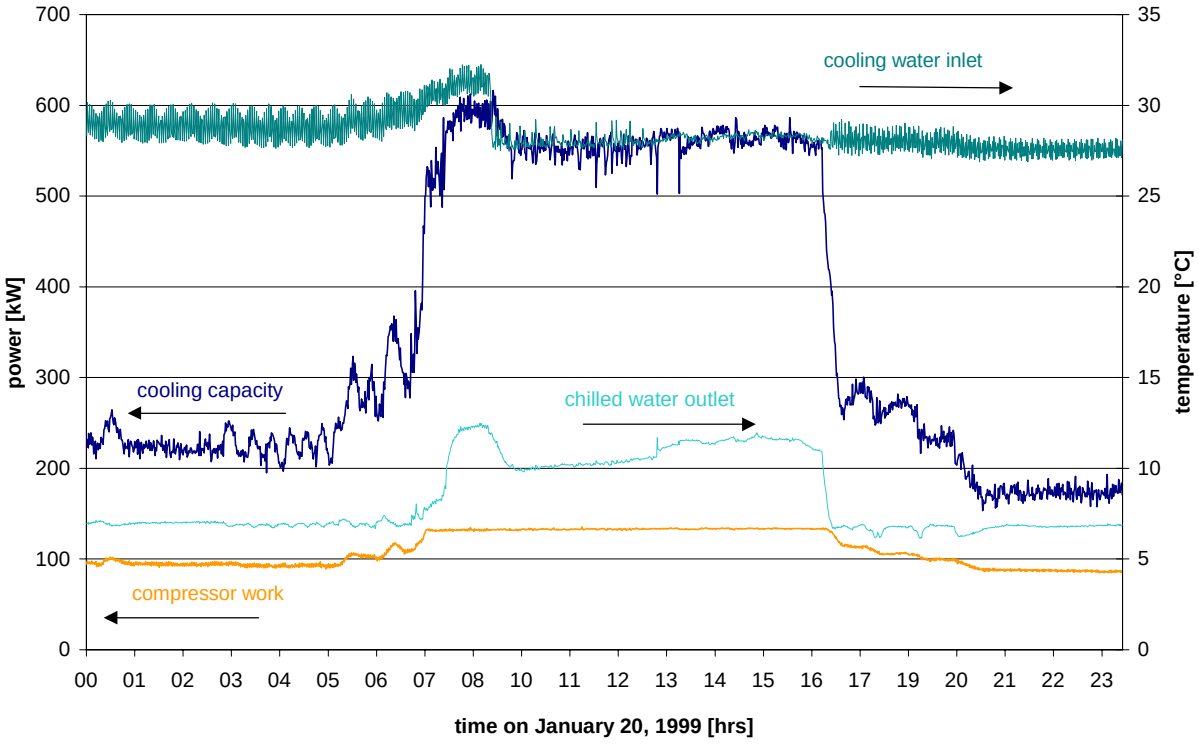

Figure 2: Operating characteristic on January 20, 1999 for Chiller A

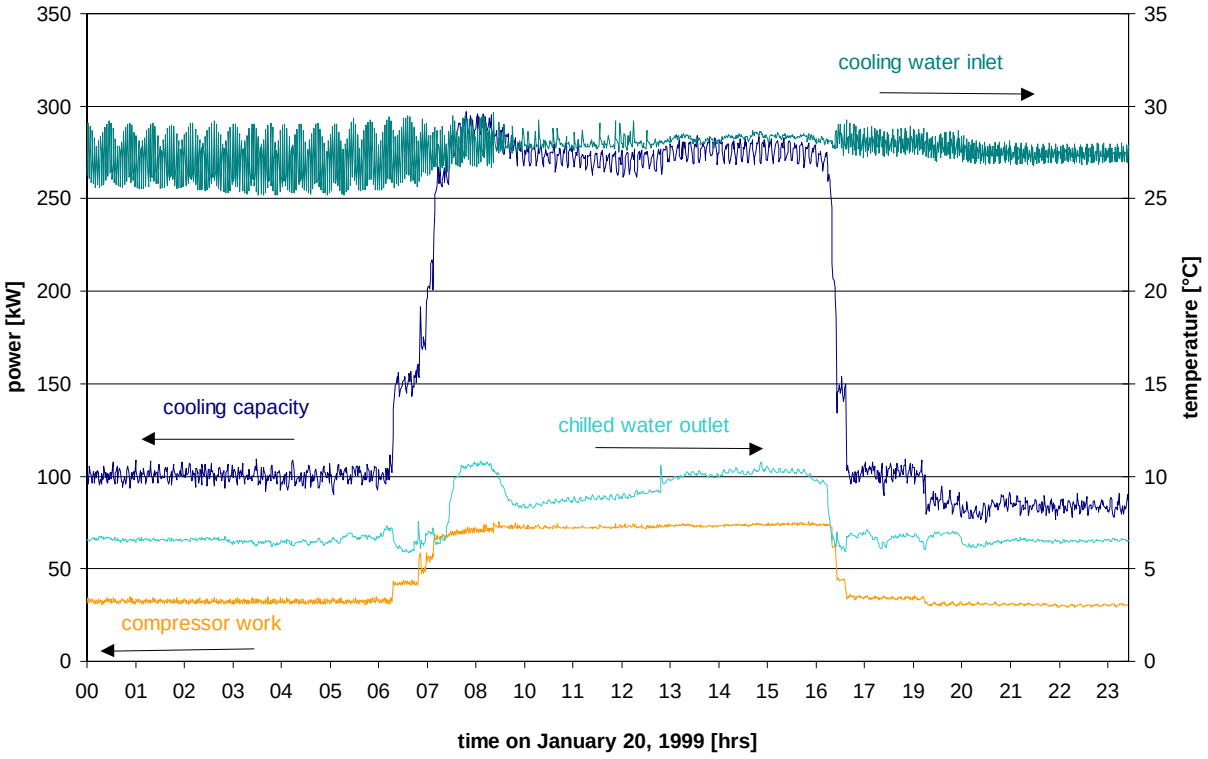

Figure 3: Operating characteristic on January 20, 1999 for Chiller B

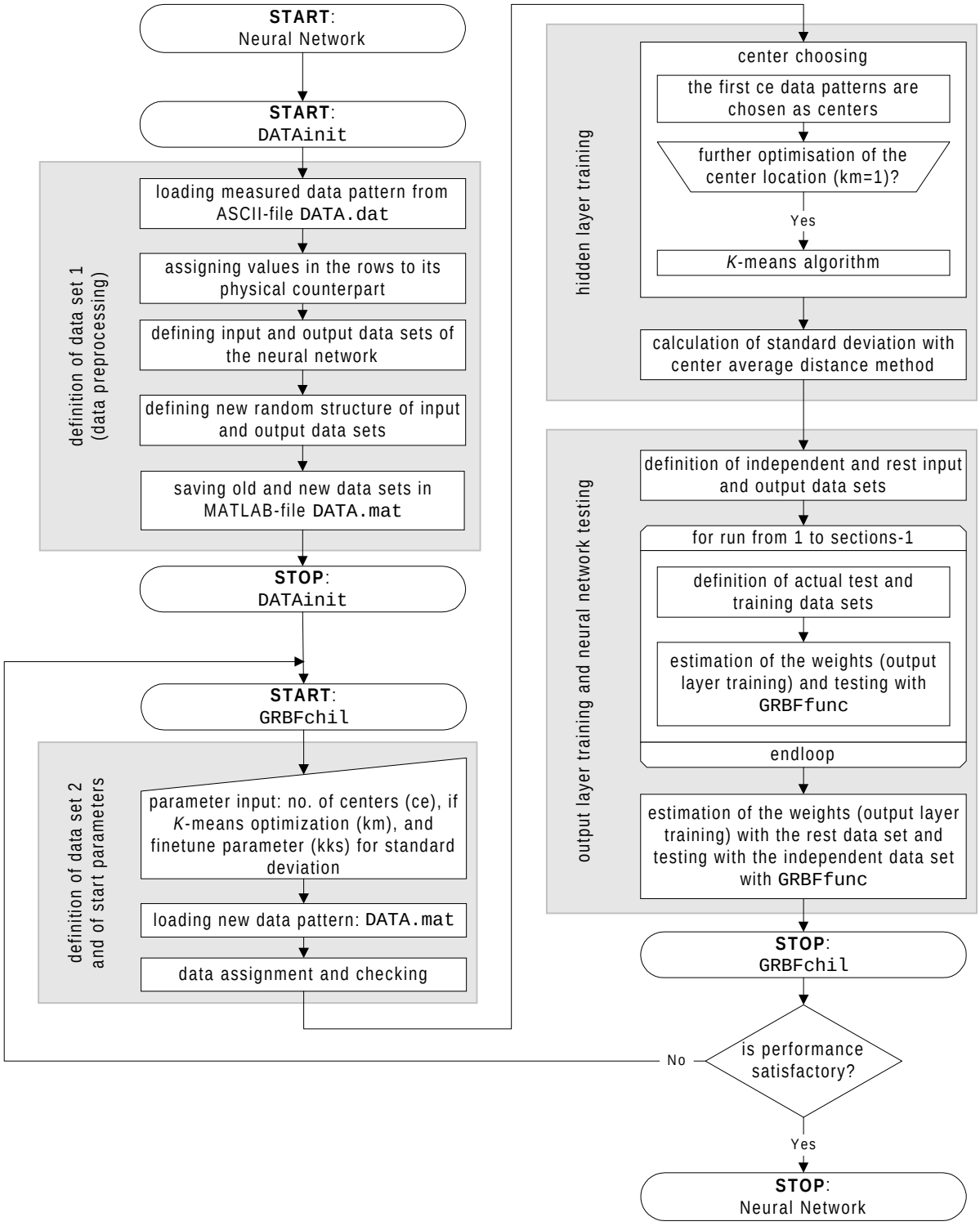

Figure 4: Flowchart of the general structure of the GRBF chiller model

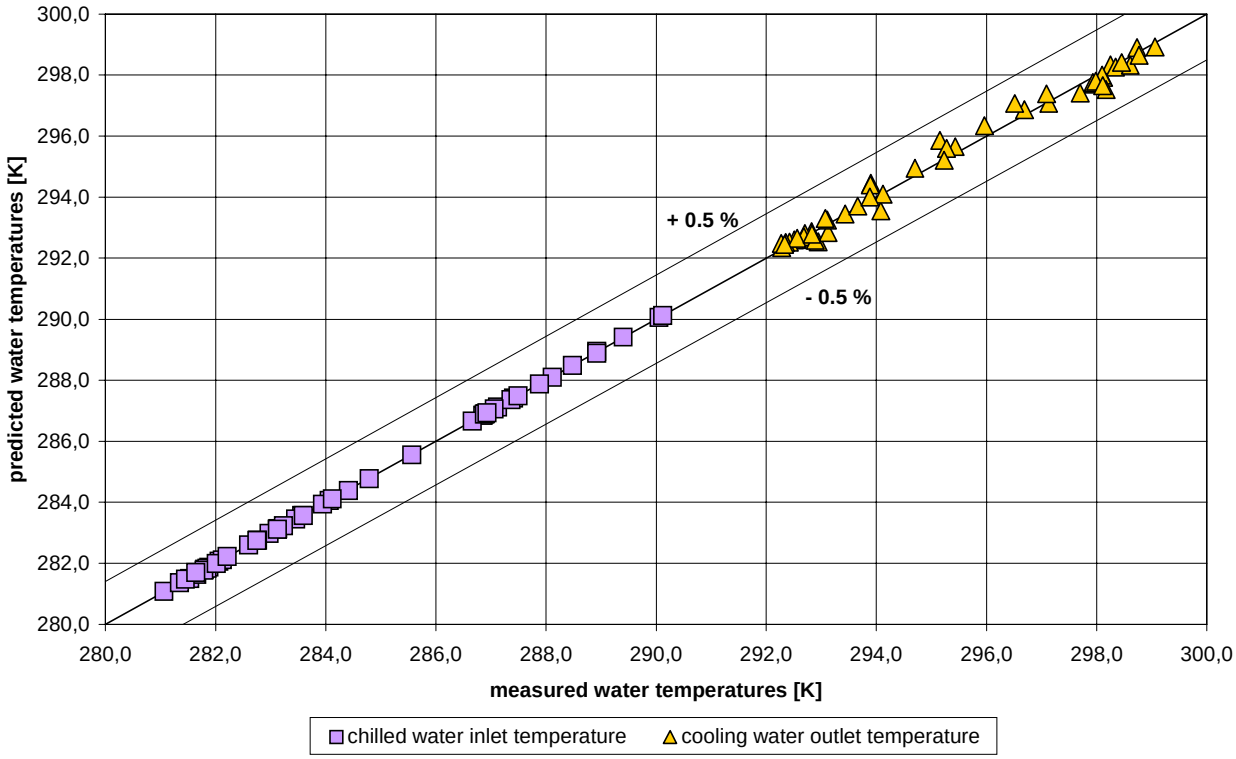

Figure 5: Comparison of predicted and measured water temperatures for Chiller A

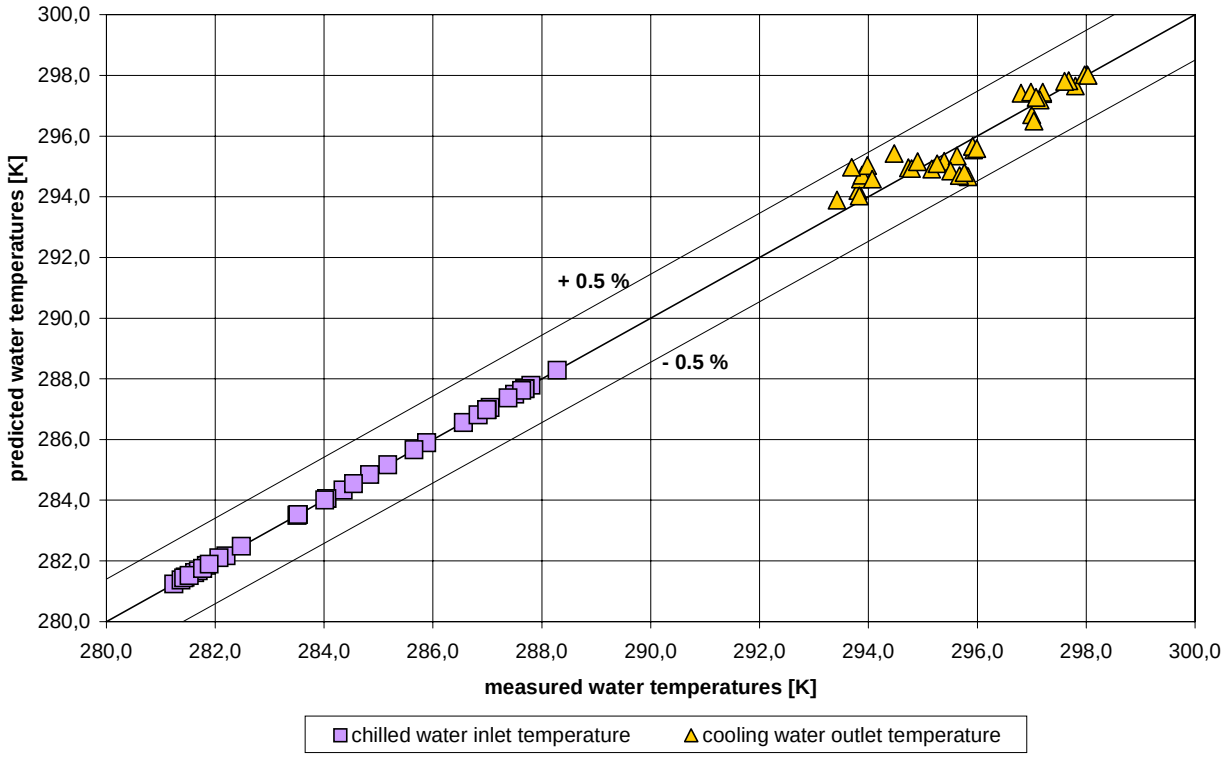

Figure 6: Comparison of predicted and measured water temperatures for Chiller B

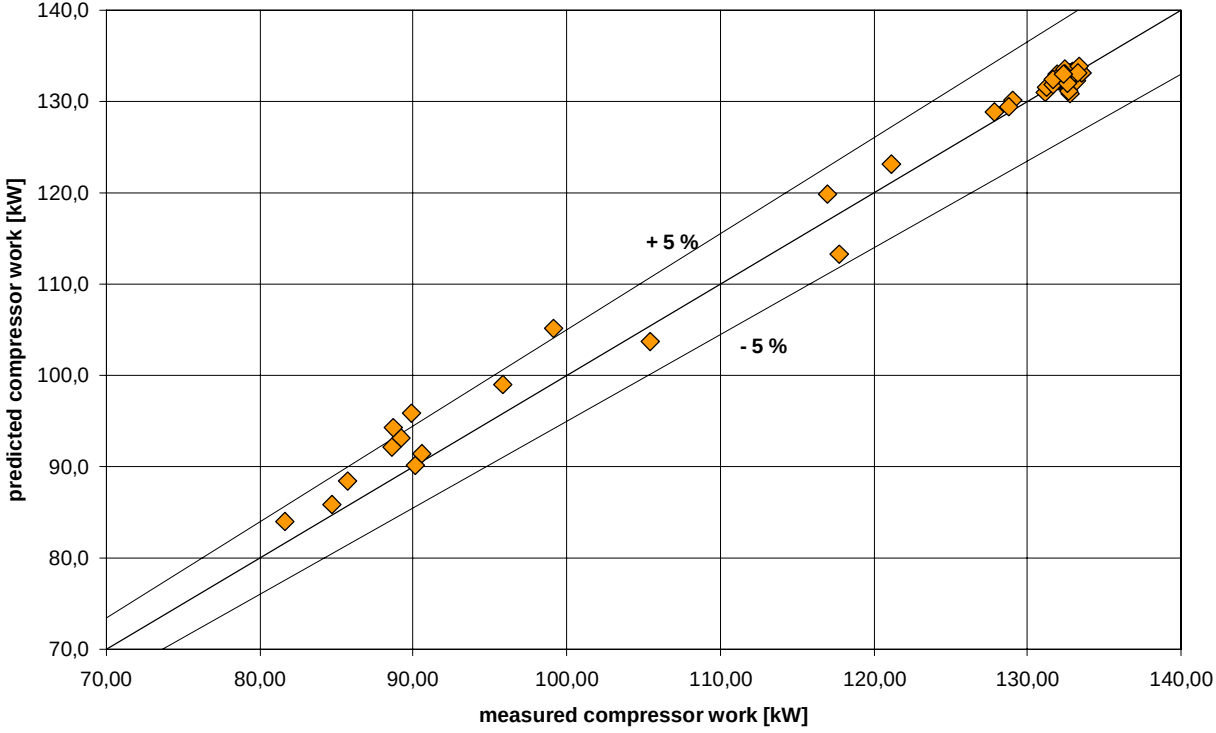

Figure 7: Comparison of predicted and measured compressor work for Chiller A

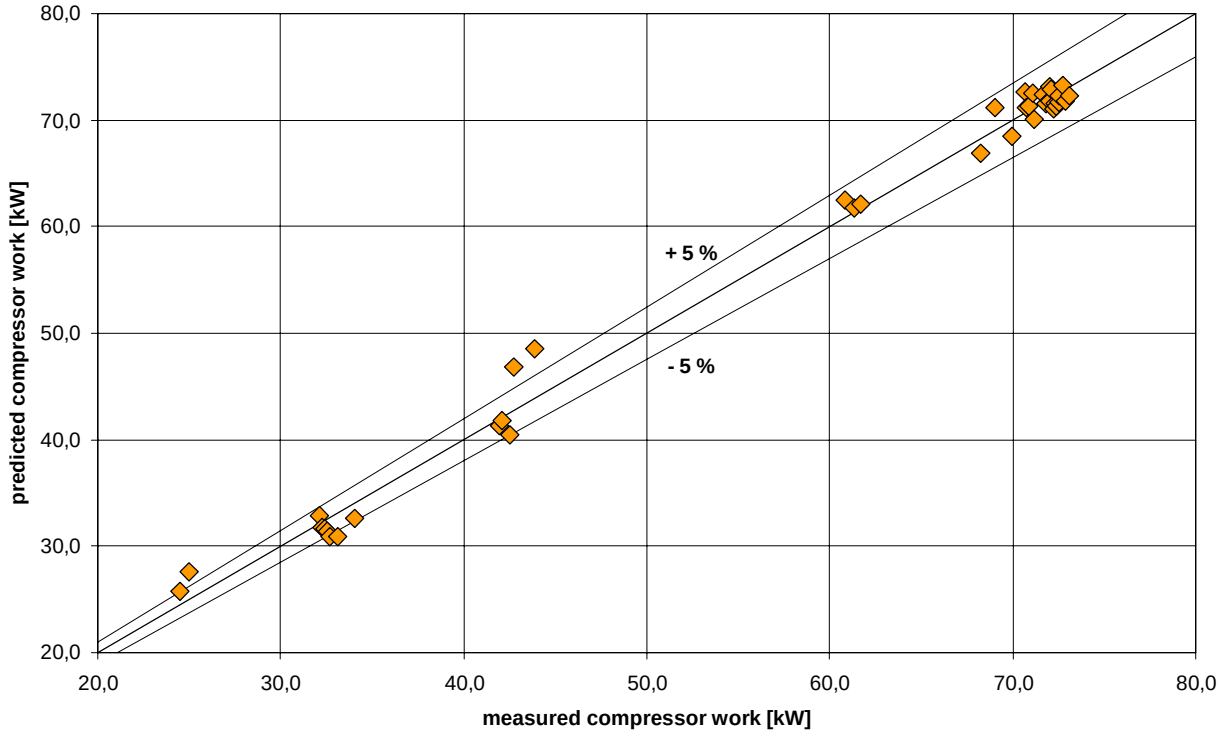

Figure 8: Comparison of predicted and measured compressor work for Chiller B

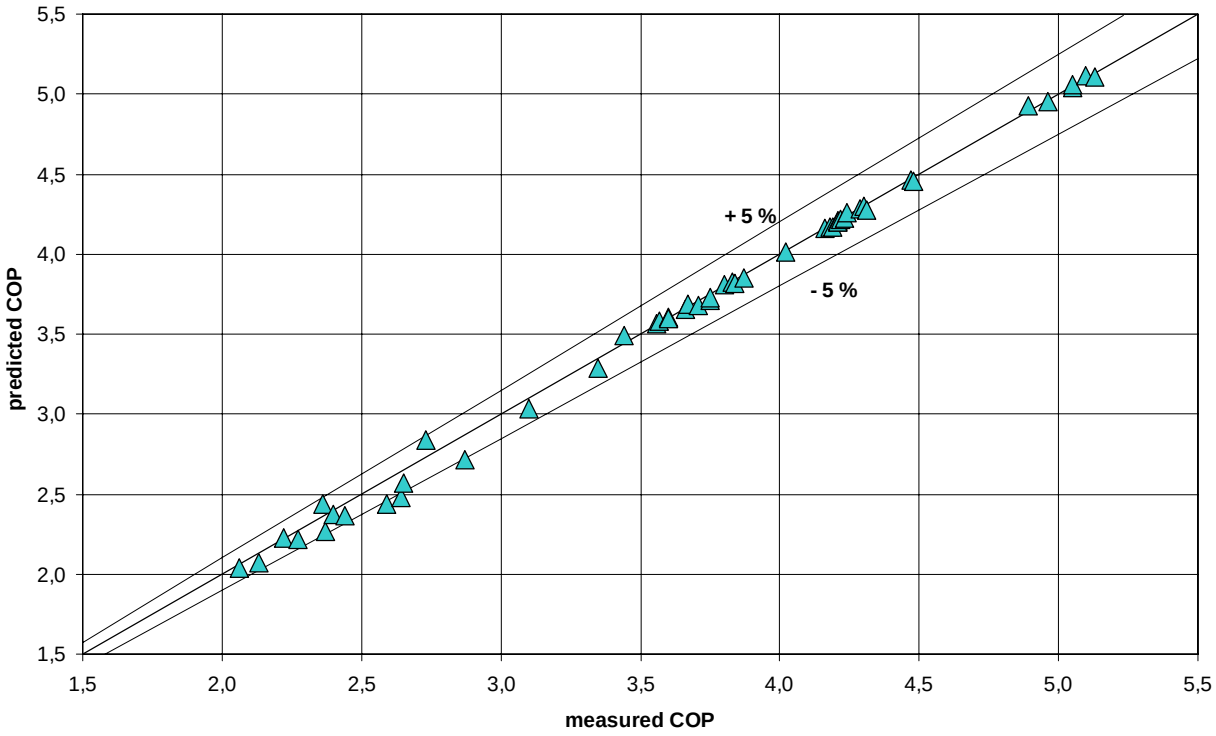

Figure 9: Comparison of predicted and measured COP for Chiller A

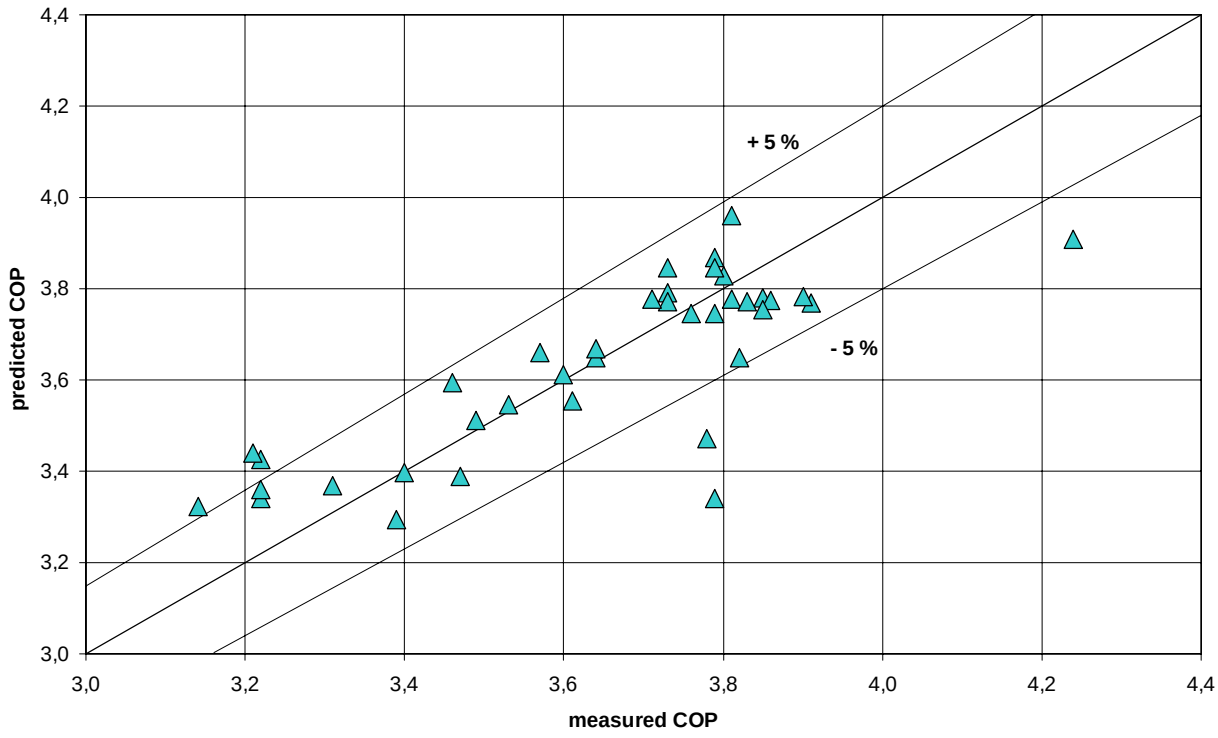

Figure 10: Comparison of predicted and measured COP for Chiller B

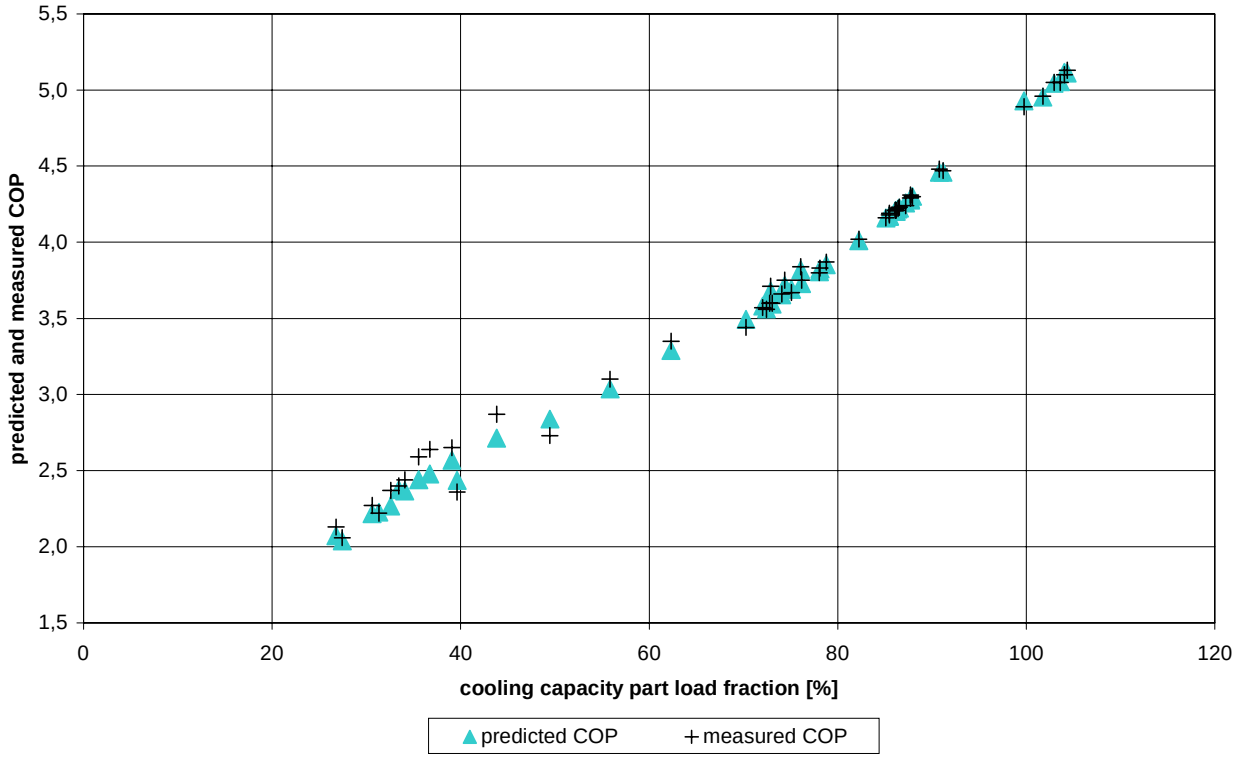

Figure 11: Comparison of predicted and measured COP over cooling capacity part load fraction for Chiller A

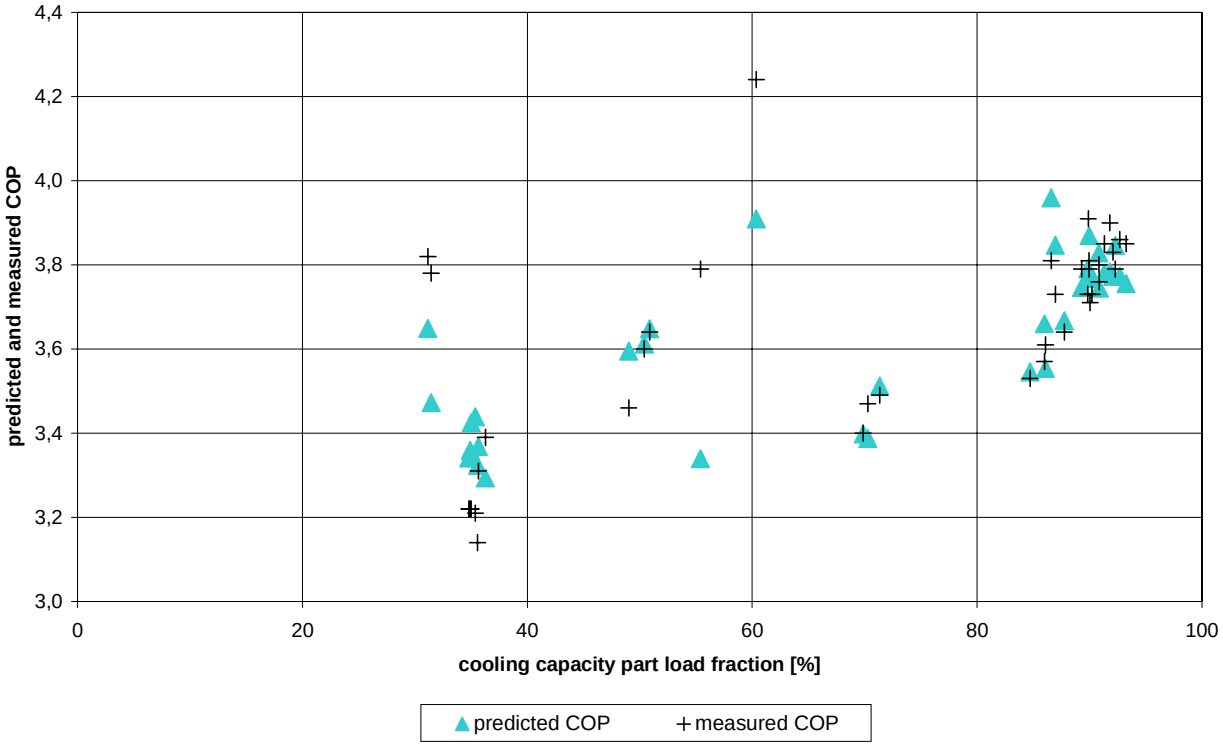

Figure 12: Comparison of predicted and measured COP over cooling capacity part load fraction for Chiller B